

Imprint of transient electron localization in H_2^+ using circularly-polarized laser pulse

Jianghua Luo(罗江华), Jun Li(李军), and Huafeng Zhang(张华峰)
Citation: Chin. Phys. B, 2020, 29 (**12**): 123201. DOI: 10.1088/1674-1056/abbbe1
Journal homepage: http://cpb.iphy.ac.cn; http://iopscience.iop.org/cpb

What follows is a list of articles you may be interested in

Resonance-enhanced two-photon ionization of hydrogen atom in intense laser field investigated by Bohmian-mechanics

Yang Song(宋阳), Shu Han(韩姝), Yu-Jun Yang(杨玉军), Fu-Ming Guo(郭福明), Su-Yu Li(李苏宇)
Chin. Phys. B, 2020, 29 (**9**): 093204. DOI: 10.1088/1674-1056/aba09e

Relative phase-dependent two-electron emission dynamics with two-color circularly polarized laser fields

Tong-Tong Xu(徐彤彤), Lian-Lian Zhang(张莲莲), Zhao Jin(金钊), Wei-Jiang Gong(公卫江)
Chin. Phys. B, 2020, 29 (**9**): 093202. DOI: 10.1088/1674-1056/ab928c

Photoelectron imaging on vibrational excitation and Rydberg intermediate states in multi-photon ionization process of NH_3 molecule

Ya-Nan Sun(孙亚楠), Yan-Hui Wang(王艳辉), Le-Le Song(宋乐乐), Hai-Bin Du(杜海滨), Xiao-Chun Wang(王晓春), Lan-Lai He(赫兰海), Si-Zuo Luo(罗嗣佐), Qin Yang(杨钦), Jing Leng(冷静), Fu-Chun Liu(刘福春)
Chin. Phys. B, 2020, 29 (**9**): 093201. DOI: 10.1088/1674-1056/ab9431

Bohmian trajectory perspective on strong field atomic processes

Xuan-Yang Lai(赖炫扬), Xiao-Jun Liu(柳晓军)
Chin. Phys. B, 2020, 29 (**1**): 013205. DOI: 10.1088/1674-1056/ab5c0f

Backward rescattered photoelectron holography in strong-field ionization

Fujun Chen(陈富军), Ruxian Yao(姚汝贤), Jianghua Luo(罗江华), Changqing Wang(王长清)
Chin. Phys. B, 2018, 27 (**10**): 103202. DOI: 10.1088/1674-1056/27/10/103202

Imprint of transient electron localization in H_2^+ using circularly-polarized laser pulse*

Jianghua Luo(罗江华)[1,2,†], Jun Li(李军)[1], and Huafeng Zhang(张华峰)[1]

[1] School of Physics and Optoelectronic Engineering, Yangtze University, Jingzhou 434023, China
[2] National Mobile Communications Research Laboratory, Southeast University, Nanjing 210096, China

(Received 31 July 2020; revised manuscript received 14 September 2020; accepted manuscript online 28 September 2020)

Photoelectron momentum distribution of hydrogen molecular ion in a circularly polarized laser pulse is calculated by solving the three-dimensional time-dependent Schrödinger equation (3D-TDSE). At the intermediate internuclear distance, an unusual multi-peak structure is observed in the angular distribution, which is proved to be a signature of the transient localization of the electron upon alternating nucleus. By tracing the time-dependent ionization rate and bound state populations, we provide a clear evidence that the transient electron localization still exists in circularly polarized pulse and the corresponding multiple ionization bursts are directly mapped onto observable angular distributions. In addition, we introduce an intuitive strong-field approximation model which incorporates laser-induced subcycle internal electron dynamics to isolate the effect of the Coulomb potential of the parent ions. In this way, the timing of each ionization burst can be directly read out from the angular distributions. Our results suggest that the ionization time serves as a sensitive tool encoding intramolecular electron dynamics and can be measured using attoclock technique.

Keywords: strong-field ionization, ultrafast phenomena, photoelectron spectrum

PACS: 32.80.Rm, 31.90.+s, 32.80.Fb **DOI:** 10.1088/1674-1056/abbbe1

1. Introduction

Various strong-field phenomena are induced or initiated by the release of an electron from the parent atoms or molecules through tunneling, known as tunneling ionization. The tunneling process in intense laser fields is often well understood in terms of quasi-static tunneling ionization picture,[1,2] characterized by an asymptotically small Keldysh parameter $\gamma \ll 1$,[3] where $\gamma = \omega\sqrt{2I_p}/E$, ω is the laser angular frequency, E_0 the amplitude of the laser electric field, and I_p the ionization potential. According to this intuitive picture, the electron releases from the bound state via tunneling through the quasi-static potential barrier formed by the laser field and the Coulomb potential of the core, thus it is expected that the instantaneous tunneling ionization rate reaches its maximum at laser maxima and exhibits a single maximum during each half cycle of the laser field.[4] However, recent results of numerical simulations on the simplest molecular system H_2^+ have shown that ionization no longer occurs at the peak of the electric field. Instead, there are multiple ionization bursts (MIBs) within one half laser cycle,[5,6] which contradicts the quasi-static tunneling picture. Time-resolved analysis has demonstrated that the MIBs are related to transient electron localization (TEL) on one of the molecular centers on sub-cycle time scale.[7,8] This laser-induced intramolecular dynamics creates charge oscillations between two nuclei, which shift the timing of ionization relative to the peak of the laser field.

Theoretical justification of TEL and the corresponding MIBs relies on the analysis of time-dependent electron density distribution in H_2^+ or alternatively the use of Bohmian trajectories.[9] However, none of them are experimentally accessible observable signals. Several schemes have been proposed to detect such nonadiabatic behavior inside the molecule. For example, the laser-induced TEL leads to a rapidly varying asymmetry of the electron density. By applying a second attosecond laser pulse polarized parallel to the molecular axis, the asymmetry of the electron density is mapped onto the asymmetry of the photoelectron momentum distribution (PMD), which could be measured experimentally in principle.[5,10] Alternatively, it has been shown that if the polarization direction of the second attosecond pulse is perpendicular to the molecular axis, the molecular single-photon ionization works as a natural double-slit experiment.[11–13] The asymmetry originating from TEL inside H_2^+ modulates the two "slits" of photoionization, leading to varying visibility of the interference fringes in the angle-resolved PMDs. In this way, the electron motion in the molecule is directly mapped out by measuring the interference visibility. Both methods are not experimentally demonstrated due to the low intensity and low repetition rate of the current attosecond laser sources. An alternative way of probing TEL is using high harmonic spectroscopy. It has been found that the TEL results in a minimum of the high harmonic spectra, whose position is separated with

*Project supported by the National Key Research and Development Program of China (Grant No. 2018YFB1801904), the National Natural Science Foundation of China (Grant No. 12075036), and the Open Research Fund of National Mobile Communications Research Laboratory, Southeast University (Grant No. 2019D14).

†Corresponding author. E-mail: jhluo09@qq.com

© 2020 Chinese Physical Society and IOP Publishing Ltd

structural interference minima.[14,15] However, it is not clear whether the minima caused by TEL can survive the macroscopic propagation effects. Thus it is still a big challenge to probe the signal of MIBs and characterize TEL.

In this paper, we propose to probe MIBs using the attosecond angular streaking technique, also known as attoclock.[16–18] The angular streaking cameras have been employed to revealing many interesting strong-field phenomena, such as measuring the tunneling time delay of ionization.[19,20] In our strategy, the prototypical H_2^+ molecular ion is tunneling ionized by a circularly polarized laser field. The TEL inside H_2^+ shifts the timings of ionization relative to the laser maxima. Several discrete bursts of ionization are angularly streaked to different directions, resulting in nonuniform PMD in the toroidal direction. Thus the signals of MIBs are directly mapped onto the photoelectron momentum distribution. The aim of this work is threefold. First, complementary to the previous prediction of TEL and MIBs in linearly and circularly polarized laser fields, we provide a clear evidence about the existence of TEL inside molecules in circularly polarized laser fields by tracing the time-dependent ionization rate and bound state populations. Previously the signature of coupling between the ground and the first excited states was predicted from the lateral PMDs in circularly-polarized laser pulse.[21] Here we demonstrate it from the PMD in the polarization plane. Second, the photoelectron angular distribution shows clear variations, which is found to be a signature of MIBs. Third, during the interaction of molecules with circularly polarized laser fields, the Coulomb interaction between a liberated electron and its parent ion would lead to an angular drift of the PMD. We thereby apply a strong field approximation (SFA) model to isolate the Coulomb effects and at the same time maintain the internal dynamics of the molecules. By this means, we correct on the amount of angular drift originated from the Coulomb interaction and the timings of MIBs can be directly read out.

2. Numerical methods

The PMDs are obtained by solving the three-dimensional (3D) time-dependent Schrödinger equation (TDSE) in Cartesian coordinates for H_2^+ with fixed internuclear distance R_0. The H_2^+ molecular ion is aligned along x axis and the laser pulse is polarized in the x–y plane. In length gauge, the TDSE within dipole approximation reads (atomic units are used unless otherwise stated)

$$\mathrm{i}\frac{\partial}{\partial t}\Psi(\boldsymbol{r},t)=\left[-\frac{\nabla^2}{2}+V(\boldsymbol{r})+\boldsymbol{r}\cdot\boldsymbol{E}(t)\right]\Psi(\boldsymbol{r},t), \tag{1}$$

where $V(\boldsymbol{r})=-1/|\boldsymbol{r}-\boldsymbol{R}_+|-1/|\boldsymbol{r}-\boldsymbol{R}_-|$ is the Coulomb potential with two nuclei located at $\boldsymbol{R}_\pm=(\pm R_0/2,0,0)$, respectively. The electric field $\boldsymbol{E}(t)$ is given by

$$\boldsymbol{E}(t) = \frac{E_0}{\sqrt{2}}\cos^2\left(\frac{\pi t}{T_\mathrm{p}}\right)[\cos(\omega t+\phi)\boldsymbol{e}_x+\sin(\omega t+\phi)\boldsymbol{e}_y] \tag{2}$$

for $T_\mathrm{p}/2<t<T_\mathrm{p}/2$ with E_0, T, ω, ϕ, and T_p being the field amplitude, the optical cycle, the angular frequency, the carrier-envelope phase (CEP), and the foot-to-foot duration, respectively. In the present study, we use 800-nm laser pulse with a peak intensity of 3.0×10^{14} W/cm^2, CEP of π, and total duration of $8T$.

The time-dependent wave function is discretized on the 3D Cartesian grid and is propagated using the Fourier split-operator method.[22–24] The Fourier transforms are accomplished by fast-Fourier-transform (FFT) algorithms. The 3D-FFT is parallelized using a domain-based 2D pencil decomposition strategy. Specifically, the total number of processes is separated into two groups $N=N_x\times N_y$. Accordingly, the 3D Cartesian grid is decomposed in x and y directions, resulting in N blocks where the grid points in z direction are local in every process. The initial ground state is obtained by imaginary-time propagation.

To eliminate the nonphysical boundary reflections in the simulation box, the wave function is smoothly split at each time step as

$$\begin{aligned}\Psi(\boldsymbol{r},t) &= f(r)\Psi(\boldsymbol{r},t)+[1-f(r)]\Psi(\boldsymbol{r},t)\\ &= \Psi_1(\boldsymbol{r},t)+\Psi_2(\boldsymbol{r},t),\end{aligned} \tag{3}$$

where $f(r)$ is the absorbing function which has a $\cos^{1/4}$ form. The outgoing electron wave packet $\Psi_2(\boldsymbol{r},t)$ is propagated analytically under the Volkov Hamiltonian until the end of the laser pulse

$$\begin{aligned}M(\boldsymbol{p},t_i) &= \mathrm{e}^{-\mathrm{i}\int_{t_i}^{t_f}[\boldsymbol{p}+\boldsymbol{A}(t)]^2/2\,\mathrm{d}t}\\ &\times\int\frac{\mathrm{e}^{-\mathrm{i}[\boldsymbol{p}+\boldsymbol{A}(t_i)]\cdot\boldsymbol{r}}}{(2\pi)^{3/2}}\Psi_2(\boldsymbol{r},t_i)\,\mathrm{d}\boldsymbol{r},\end{aligned} \tag{4}$$

where $\boldsymbol{A}(t)=-\int_{-\infty}^{t}\boldsymbol{E}(t')\,\mathrm{d}t'$ denotes the vector potential of the laser pulse. The final 3D PMD is obtained by gathering all the electron flux $w(\boldsymbol{p})=\left|\sum_{t_i}M(\boldsymbol{p},t_i)\right|^2$.

In our calculation, we use grid sizes of $1607\times1607\times803$, in x, y, and z directions, respectively, decomposed on a 16×16 process grid (the total number of processes is 256). The spatial box covers ±153 a.u. in x and y dimensions, and ±84.5 a.u. in z dimension. The decomposition is done using the open-source 2DECOMP&FFT library.[25] The positions of the two nuclei are displaced with respect to the grid points in order to avoid the singularity of the Coulomb potential. The time step is 0.05 a.u. After the end of the laser pulse, the propagation is continued for additional 4 optical cycles to ensure that the ionized and the bound parts of the wave function are well separated.

3. Results and discussion

Firstly, the principle of probing TEL using angular streaking camera is sketched in Fig. 1. The electric field of the circularly polarized laser pulse is presented in Fig. 1(a) by green curves. The laser polarization rotates counter-clockwise and the molecular axis of H_2^+ is horizontal. According to the quasi-static tunneling picture, when the Coulomb potential is neglected, the ionization rate is expected to be the largest when the electric field is aligned along the molecular axis. Therefore, the asymptotic momentum distribution of photoelectrons is expected to peak perpendicular to the molecular axis on a ring with a radius equal to the amplitude of the laser vector potential. However, the laser-induced transient localization of the bound electron changes the time of peak ionization and there are multiple ionization bursts near the peak of the laser field, as indicated by the arrows. According to the relation between the asymptotic momentum and the ionization time $\boldsymbol{p} = -\boldsymbol{A}(t_i)$, these ionization bursts are angularly streaked to different directions, resulting in a more complex angular structure as shown in Fig. 1(b).

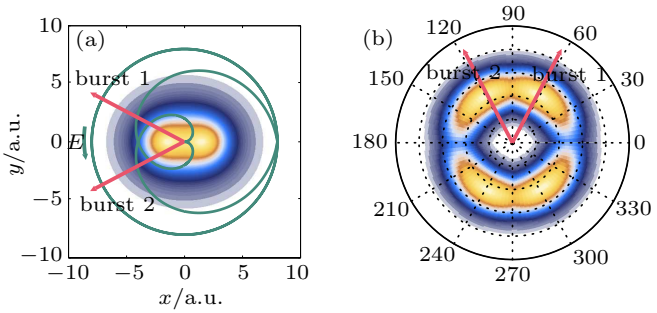


Fig. 1. (a) Electric field of the circularly polarized laser pulse rotating counterclockwise and the ground state wave function of H_2^+, aligned along x axis. The two arrows indicate two times of the transient electron localization in one half cycle of the laser field. (b) The photoelectron momentum distribution without including the Coulomb action on the tunneled electron. The arrows indicate the maxima induced by the two ionization bursts. The momentum distribution is calculated using the strong field approximation model with the intramolecular electron dynamics included. This method will be illustrated below in detail. Here only one cycle of the laser pulse is used in the calculations.

Next, we present the PMDs obtained by solving TDSE. Here, we focus on the 2D PMDs in the polarization plane of the laser pulse, calculated by $Y(p_x, p_y) = \int_{-0.2}^{0.2} w(\boldsymbol{p})\,\mathrm{d}p_z$. Figure 2(a) shows 2D PMD of H_2^+ at equilibrium internuclear distance 2 a.u. The wavelength of the laser pulse is 800 nm and the intensity is 3.0×10^{14} W/cm^2. The peak of PMD tilts counterclockwise, in the same direction as the rotation of the laser field. The angular drift of PMD can be clearly viewed in the energy-integrated angular distribution, as shown in Fig. 2(b). Previous studies have shown that this angular drift is due to the influence of the Coulomb effect of the parent ion.[26] The Coulomb interaction distorts the motion of the ionized electron wavepackets after tunneling, thus the asymptotic momentum distribution of photoelectrons exhibits non-negligible offset angles with respect to the prediction of quasi-static tunneling theories.[26–31] Figure 2(c) presents the PMD of H_2^+ for an internuclear separation of 4 a.u. Besides the overall angular shift, a more complex angular structure of PMD appears. There are two maxima in the momentum distribution on the upper half plane. The PMD is energy-integrated and the resulted angle-resolved distribution is shown in Fig. 2(d). Two maxima, peak A at 152° and peak B at 80°, can be clearly observed.

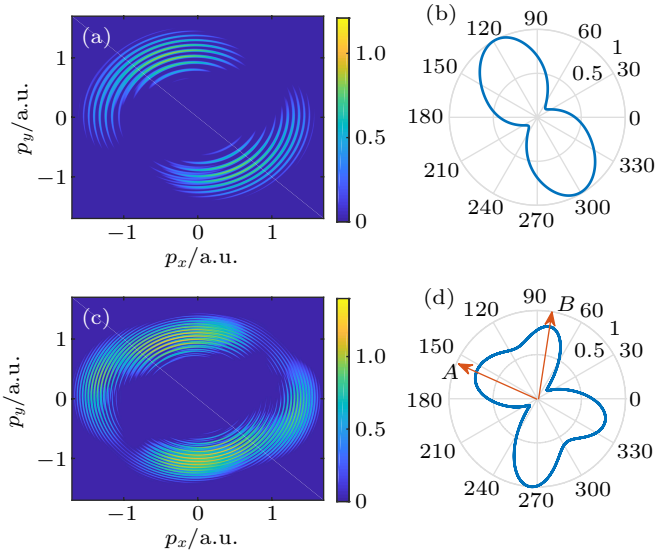


Fig. 2. The 2D PMDs for H_2^+ in the polarization plane at internuclear distance (a) $R_0 = 2$ a.u. and (c) $R_0 = 4$ a.u. (b) and (d) The energy-integrated angular distribution corresponding to (a) and (c), respectively. The two maxima of the angle-resolved final momentum distribution in (d) are marked by A and B. We use an 800-nm circularly polarized laser pulse with an intensity of 3.0×10^{14} W/cm^2.

In order to explore the physical origin of the angular variation of PMD of H_2^+ at $R = 4$ a.u., we calculate the instantaneous ionization rate. The time-dependent ionization rate is defined as $\mathrm{d}P_{\mathrm{ion}}(t)/\mathrm{d}t$, where $P_{\mathrm{ion}}(t)$ is the population of ionized electrons. $P_{\mathrm{ion}}(t)$ is obtained by projecting out the bound states, i.e., $P_{\mathrm{ion}}(t) = 1 - \sum_i |c_i|^2$, where $|c_i|^2$ is the time-dependent bound-state population. Here the lowest-lying five bound states are included. The time-dependent bound-state populations are recorded during the propagation in the laser fields. The ionization rate is shown in Fig. 3(b). Since the transition dipole between the $1s\sigma_g$ and $2p\sigma_u$ states is strongly aligned along the molecular axis. Therefore, effectively only the parallel component of the field is important. Figure 3(a) shows the laser component along the molecular axis in the middle part of the laser pulse. We focus on the behavior of the ionization rate in one optical cycle $[-0.75T, 0.25T]$. There are two ionization peaks per half cycle, marked by A, B and A', B', a clear signature of MIBs in molecules. Hence we show that the MIBs exist not only in linearly but also in circularly polarized laser fields. According to the angular streaking principle, the two ionization bursts are angularly streaked into different directions, thus the two peaks A and B of the angle-resolved

momentum distribution in Fig. 2(d) are the imprints of ionization bursts A and B in Fig. 3(b), respectively.

Next, we will demonstrate that the MIBs are induced by the subcycle TEL inside the molecule by tracing the field-driven bound-state dynamics during propagation. This is done by recording time-dependent populations $|c_i(t)|^2 = |\langle i|\Psi(t)\rangle|^2$ of ground $1s\sigma_g$ ($|g\rangle$) and first excited $2p\sigma_u$ ($|u\rangle$) states of H_2^+ during the propagation in the laser fields, where $c_i(t)$ ($i = g,u$) are the projection coefficients and $\Psi(t)$ is the full time-dependent wavefunction calculated by solving the TDSE. Here only the two lowest-lying states are adopted, because for a two-center system as H_2^+, the ground and the first excited states are adequate to capture the main feature of election oscillation inside the molecule. The truncated bound part of the electron wave function is expressed as

$$\psi_b(t) = c_g(t)|g\rangle + c_u(t)|u\rangle. \tag{5}$$

The electron density distribution as a function of time along the molecular axis, integrated over y and z directions, is presented in Fig. 3(c). One can see that within per half cycle, the electron transiently localizes on one of the two protons two times. Specially, one of the local electron density maxima appears before the peak of the laser field and the second one is localized after the laser peak. The positions of the local electron density maxima coincide with those of the ionization bursts, as guided by the vertical lines. Small discrepancy can be due to the excitation of the higher-lying excited states.[32] This result confirms that the MIBs are indeed induced by the subcycle TEL inside the molecule. Previously, TEL is found to occur in linearly polarized laser fields for H_2^+ at intermediate internuclear distance. Here we unambiguously demonstrate that the TEL and MIBs still exist in circularly polarized laser fields. Furthermore, we show that the signature of MIBs is mapped onto the photoelectron angular distribution, which can be measured experimentally. In our calculation, we use a fixed internuclear distance. However in reality the vibrational motion of the nuclear wave packet will lead to different molecular configurations at the different maxima of the electric field. In experiment, the internuclear distance at the instant of ionization can be determined from the kinetic energy release of the protons[26] using the cold-target recoil-ion-momentum spectroscopy (COLTRIMS) technique. Thus photoelectrons belonging to certain molecular configurations can be determined.

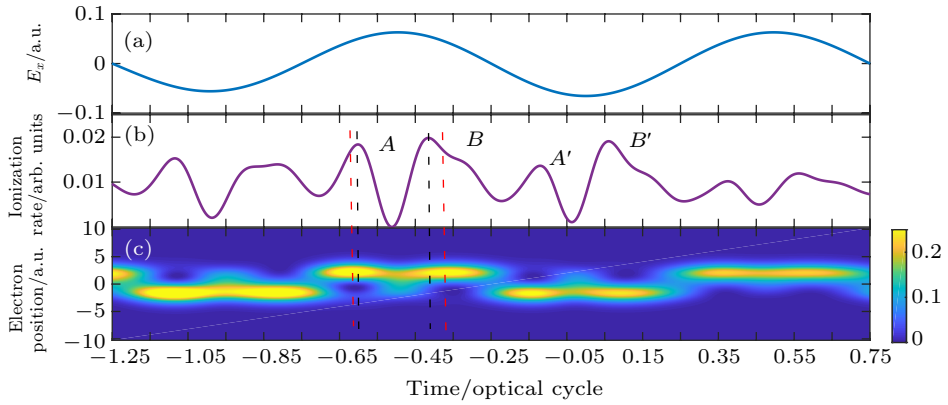


Fig. 3. (a) Laser field component along the molecular axis in the middle part from $-1.25T$ to $0.75T$. (b) Time-dependent ionization rate of H_2^+ at $R = 4$ a.u. The ionization peaks in the first cycle are marked by A, B and A', B'. The vertical black dashed lines indicate the positions of peaks A and B to guide the eye. (c) Time evolution of the bound state electron density distribution along the molecular axis. The vertical red dashed lines indicate the position of transient local maxima. Laser parameters are the same as those in Fig. 2.

In comparison with the expected PMD shown in Fig. 1(b), the PMD obtained by solving the TDSE shows an overall counter-clockwise angular drift in Fig. 2(c), due to the influence of the Coulomb potential. This angular drift prevents evaluating the timing of MIBs from the angle-resolved PMD. Previously, the Coulomb effects on the angular distribution of photoelectron have been studied by screening the Coulomb potential with a mask function numerically.[33] In the following, we will develop a method to exclude the Coulomb effect and at the same time maintain the pre-ionization intramolecular electron dynamics within the framework of SFA.[34,35] The modification of SFA for molecules has been extensively studied and developed with detailed derivation and justification on solid mathematical foundations.[36,37] We begin with the Dyson integral

$$\mathcal{M}(\boldsymbol{p}) = -\mathrm{i}\int_0^{T_p} \mathrm{d}t\mathcal{D}(\boldsymbol{p},t), \tag{6}$$

which gives the photoelectron momentum distribution $|\mathcal{M}(\boldsymbol{p})|^2$. The integrand is given by

$$\mathcal{D}(\boldsymbol{p},t) = \langle\psi_{\boldsymbol{p}}^{(-)}|\hat{U}(T_p,t)V_L(t)\hat{U}_0(t,0)|\psi_i\rangle, \tag{7}$$

where $\hat{U}_0(t,0)$ denotes the field-free time-evolution operator of Hamiltonian H_0 and $\hat{U}(T_p,t)$ the full time-evolution operator of Hamiltonian $H(t)$. According to SFA, the scattering state $\langle\psi_{\boldsymbol{p}}^{(-)}|$ is replaced by a plane wave $\langle\boldsymbol{p}|$ and the full time evolution operator $\hat{U}(T_p,t)$ is approximated by

the Volkov time-evolution operator $\hat{U}_{\rm V}(T_{\rm p},t)$ of Hamiltonian $-\frac{1}{2}\nabla^2+V_{\rm L}(t)$, which neglects the Coulomb potential. This leads to the transition amplitude

$$\mathcal{M}_{\rm SFA}(\boldsymbol{p})=-{\rm i}\int_0^{T_{\rm p}}M(\boldsymbol{p},t)\exp[-{\rm i}S(\boldsymbol{p},t)]\,{\rm d}t, \tag{8}$$

with the action

$$S(\boldsymbol{p},t)=\int_t^T\frac{[\boldsymbol{p}+\boldsymbol{A}(\tau)]^2}{2}\,{\rm d}\tau \tag{9}$$

and the transition matrix element

$$M(\boldsymbol{p},t)=\langle\boldsymbol{p}+\boldsymbol{A}(t)|\boldsymbol{r}\cdot\boldsymbol{E}(t)|\psi_i(t)\rangle. \tag{10}$$

Here, in order to include the pre-ionization bound electron dynamics, we approximate $\psi_i(t)$ by the truncated bound state in Eq. (5), i.e., $\psi_{\rm i}(t)\approx\psi_{\rm b}(t)$. Then the transition matrix element becomes

$$\begin{aligned}M(\boldsymbol{p},t)\;=\;&c_g(t)\langle\boldsymbol{p}+\boldsymbol{A}(t)|\boldsymbol{r}\cdot\boldsymbol{E}(t)|g\rangle\\&+c_u(t)\langle\boldsymbol{p}+\boldsymbol{A}(t)|\boldsymbol{r}\cdot\boldsymbol{E}(t)|u\rangle,\end{aligned} \tag{11}$$

where the time-dependent coefficients $c_g(t)$ and $c_u(t)$ are obtained from the TDSE calculations. We would like to notice that these two coefficients can also be evaluated by a two-state model, in which the time evolution of the wavefunction in the laser field is described in the basis of Floquet states.[38,39] Equation (11) is the central equation of our reformulated SFA method, which can be recognized as SFA equations coupling the dressed bound-state wave packet $\psi_{\rm b}(t)$ to a flat (plane wave) continuum. Here the effect of ionization is treated twice, i.e., with $c_i(t)$ taken from TDSE calculations and SFA transition matrix element $\langle\boldsymbol{p}+\boldsymbol{A}(t)|\boldsymbol{r}\cdot\boldsymbol{E}(t)|i\rangle$ $(i=g,u)$. In order to avoid this problem, the SFA transition matrix element is renormalized. The SFA amplitude $\mathcal{M}_{\rm SFA}(\boldsymbol{p})$ is evaluated by the saddle point approximation by replacing the integral with a discrete sum over stationary points of the action. The result is

$$\begin{aligned}\mathcal{M}_{\rm SFA}(\boldsymbol{p})\;=\;&-\sum_{t_{\rm s}^g}c_g[{\rm Re}(t_{\rm s}^g)]\langle\boldsymbol{p}+\boldsymbol{A}(t_{\rm s}^g)|\boldsymbol{r}|g\rangle\boldsymbol{E}(t_{\rm s}^g)\\&\times\sqrt{\frac{2\pi}{{\rm i}S''(\boldsymbol{p},t_{\rm s}^g)}}\exp[-{\rm i}S(\boldsymbol{p},t_{\rm s}^g)]\\&-\sum_{t_{\rm s}^u}c_u[{\rm Re}(t_{\rm s}^u)]\langle\boldsymbol{p}+\boldsymbol{A}(t_{\rm s}^u)|\boldsymbol{r}|u\rangle\boldsymbol{E}(t_{\rm s}^u)\\&\times\sqrt{\frac{2\pi}{{\rm i}S''(\boldsymbol{p},t_{\rm s}^u)}}\exp[-{\rm i}S(\boldsymbol{p},t_{\rm s}^u)].\end{aligned} \tag{12}$$

Here $t_{\rm s}^{g/u}$ are complex ionization times satisfying

$$[\boldsymbol{p}+\boldsymbol{A}(t_{\rm s}^{g/u})]^2/2+|E_{g/u}|=0, \tag{13}$$

where E_g and E_u are the bound energies of the $1s\sigma_{\rm g}$ and $2p\sigma_{\rm u}$ states, respectively.

In Fig. 4(a), we show the PMD calculated using SFA without bound state dynamics, i.e., $\psi_i(t)=|g\rangle\exp(-{\rm i}E_gt)$. In this case, the present simulation becomes equivalent to the plain SFA. The asymptotic electron momentum peaks perpendicular to the molecular axis, as expected by the conventional SFA. In Figs. 4(b) and 4(c), we present the PMD and the energy-integrated momentum distribution with the influence of the Coulomb potential removed using the SFA theory Eqs. (12) and (13), which can be compared to Figs. 2(c) and 2(d). Figure 4(b) shows the PMD with bound state dynamics. The distribution exhibits a clear two-peak structure in the upper half plane. The two peaks are located on two sides of the p_y axis, which can be more clearly seen in the energy-integrated momentum distribution shown in Fig. 4(c). Quantitatively, the two peaks A and B in Fig. 4(c) locate at 120° and 59°, respectively. According to the attoclock technique, the relation between the asymptotic momentum and the ionization time is $\boldsymbol{p}=-\boldsymbol{A}(t_i)$. Thus, the two peaks correspond two ionization bursts with ionization timings of $-0.41T$ and $-0.59T$. In comparison with the timings $-0.41T$ and $-0.60T$ of the two peaks in Fig. 3(b), the extracting ionization times agree well with the simulated results. Therefore, the position of the two peaks coincides closely with the shift of the transient electron local maximal relative to the peak of the laser field seen in Fig. 3(b), indicating that the overall angular shift in Fig. 2(c) is subtracted by isolating the Coulomb potential. Our result shows that the "corrected" PMD allows us to directly read out the timings of the ionization burst.

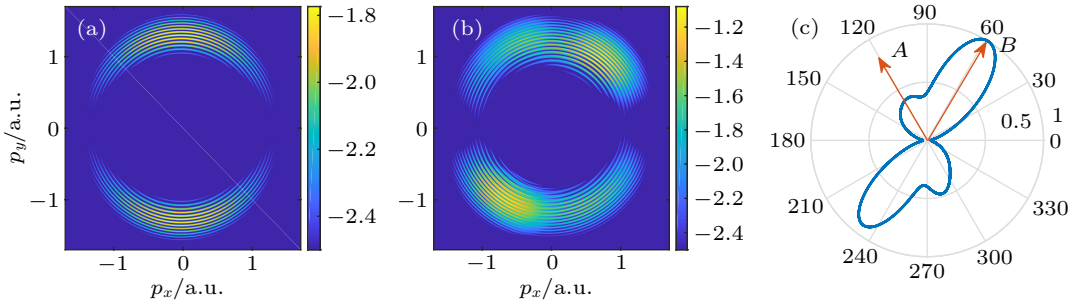


Fig. 4. (a) The PMD for H_2^+ at $R_0=4$ a.u. using SFA, in which the Coulomb potential is not taken into account and only the field-free ground state is taken into account. (b) Same as (a) but with laser-driven two-level bound-state. (c) The energy-integrated angular distribution of (b). The arrows indicate the peak positions.

4. Conclusion

In summary, we studied the tunneling ionization of H_2^+ at intermediate internuclear distance in circularly polarized laser fields. The angle-resolved photoelectron momentum distribution exhibits an unusual multi-peak structure. By tracing the time evolution of bound state wavefunctions, we found that the angular variation of PMD is induced by the transient localization of electrons inside the molecule. Thus we provided more clear evidence of the existence of TEL and the corresponding MIBs in circularly polarized laser fields. More importantly, our result indicated that the intramolecular electron dynamics on the attosecond time scale can be mapped onto experimentally accessible photoelectron momentum. Furthermore, the Coulomb potential causes an overall angular shift of the PMD, obstructing a direct extraction of the multiple ionization times. We thereby developed a method to exclude the Coulomb effects and at the same time include the dynamics of the bound electron. In this way the timings of ionization bursts can be unambiguously revealed using the attoclock technique. We would like to add a few words about the influence of the nonadiabatic effect. In all of our calculation in this manuscript, the Keldysh parameters for the lasers are a little smaller than 1. In this case, one would expect the nonadiabatic effect to occur. However, for the PMD using circularly polarized laser pulse, the nonadiabatic effect only influences the radial distribution,[40,41] whereas we focus here on the angular distribution. Thus the nonadiabatic almost has no influence on our result. This method can be used to probe intramolecular electron dynamics for other molecules, where the TEL is expected to occur at equilibrium internuclear distance.

In the present paper we only focus on the angular distribution and does not consider the interference structures in the PMD. Very recently, it has been experimentally found that for atoms the ATI rings in the PMD show distinct angular shifts, which sensitively depend on the electron energy, using near circular laser pulse.[42] So it is interesting to see if the timing information about TEL dynamics and MIBs of molecules can be extracted from the energy-resolved angular shift.

References

[1] Ammosov M V, Delone N B and Kraĭnov V P1986 *Sov. Phys. JETP* **64** 1191
[2] Delone N B and Kraĭnov V P 1991 *J. Opt. Soc. Am. B* **8** 1207
[3] Keldysh L V1965 *Sov. Phys. JETP* **20** 1307
[4] Uiberacker M, Uphues T, Schultze M, Verhoef A J, Yakovlev V, Kling M F, Rauschenberger J, Kabachnik N M, Schröder H, Lezius M, Kompa K L, Muller H G, Vrakking M J J, Hendel S, Kleineberg U, Heinzmann U, Drescher M and Krausz F 2007 *Nature* **446** 627
[5] Takemoto N and Becker A 2010 *Phys. Rev. Lett.* **105** 203004
[6] Takemoto N and Becker A 2011 *Phys. Rev. A* **84** 023401
[7] Kawata I, Kono H and Fujimura Y 1999 *J. Chem. Phys.* **110** 11152
[8] He F, Becker A and Thumm U 2008 *Phys. Rev. Lett.* **101** 213002
[9] Takemoto N and Becker A 2011 *J. Chem. Phys.* **134** 074309
[10] Miller M R, Xia Y, Becker A and Jaroń-Becker A 2016 *Optica* **3** 259
[11] Yudin G L, Chelkowski S, Itatani J, Bandrauk A D and Corkum P B 2005 *Phys. Rev. A* **72** 051401(R)
[12] Gräfe S, Engel V and Ivanov M Y 2008 *Phys. Rev. Lett.* **101** 103001
[13] Xu M H, Peng L Y, Zhang Z and Gong Q H 2011 *J. Phys. B: At. Mol. Opt. Phys.* **44** 021001
[14] Miller M R, Jaroń-Becker A and Becker A 2016 *Phys. Rev. A* **93** 013406
[15] Miller M R, Jaroń-Becker A and Becker A 2017 *Mol. Phys.* **115** 1758
[16] Eckle P, Pfeiffer A N, Cirelli C, Staudte A, Dörner R, Muller H G, Büttiker M and Keller U 2008 *Science* **322** 1525
[17] Pfeiffer A N, Cirelli C, Smolarski M, Dörner R and Keller U 2011 *Nat. Phys.* **7** 428
[18] Ivanov M and Smirnova O 2011 *Phys. Rev. Lett.* **107** 213605
[19] Torlina L, Morales F, Kaushal J, Ivanov I, Kheifets A, Zielinski A, Scrinzi A, Muller H G, Sukiasyan S, Ivanov M Y and Smirnova O 2015 *Nat. Phys.* **11** 503
[20] Camus N, Yakaboylu E, Fechner L, Klaiber M, Laux M, Mi Y, Hatsagortsyan K Z, Pfeifer T, Keitel C H and Moshammer R 2017 *Phys. Rev. Lett.* **119** 023201
[21] Abu-samha M and Madsen L B 2016 *Phys. Rev. A* **94** 023414
[22] Feit M D, Fleck J A and Steiger A 1982 *J. Comput. Phys.* **47** 412
[23] Bandrauk A D and Shen H 1993 *J. Chem. Phys.* **99** 1185
[24] Chen F J, Yao R X, Luo J H and Wang C Q 2018 *Chin. Phys. B* **27** 103202
[25] Li N and Laizet S 2010 *Cray User Group* 2010 *Conference, Edinburgh*
[26] Odenweller M, Takemoto N, Vredenborg A, Cole K, Pahl K, Titze J, Schmidt L, Jahnke T, Dörner R and Becker A 2011 *Phys. Rev. Lett.* **107** 143004
[27] Huang C, Li Z H, Zhou Y M, Tang Q B, Liao Q and Lu P X 2012 *Opt. Express* **20** 11700
[28] Martiny C, Abu-samha M and Madsen L B 2009 *J. Phys. B: At. Mol. Opt. Phys.* **42** 161001
[29] Goreslavski S P, Paulus G G, Popruzhenko S V and Shvetsov-Shilovski N I 2004 *Phys. Rev. Lett.* **93** 233002
[30] Li M, Liu Y Q, Liu H, Ning Q C, Fu L B, Liu J, Deng Y K, Wu C Y, Peng L Y and Gong Q H 2013 *Phys. Rev. Lett.* **111** 023006
[31] Shafir D, Soifer H, Vozzi C, Johnson A S, Hartung A, Dube Z, Villeneuve D M, Corkum P B, Dudovich N and Staudte A 2013 *Phys. Rev. Lett.* **111** 023005
[32] Sarkar C, Bhattacharyya S S and Saha S 2011 *J. Chem. Phys.* **134** 074309
[33] He P L, Takemoto N and He F 2015 *Phys. Rev. A* **91** 063413
[34] Sali'eres P, Carré B, Déroff L, Grasbon F, Paulus G G, Walther H, Kopold R, Becker W, Milošević D B, Sanpera A and Lewenstein M 2001 *Science* **292** 902
[35] Milošević D B, Paulus G G, Bauer D and Becker W 2006 J. Phys. B: At. Mol. Opt. Phys. **39** R203
[36] Becker W, Chen J, Chen S G and Milošević D B 2017 *Phys. Rev. A* **96** 063421
[37] Busuladžić M, Busuladžić A, Becker W and Milošević D B 2013 *Eur. Phys. J. D* **67** 61
[38] Santana A, Llorente J and Delgado V 2001 *J. Phys. B: At. Mol. Opt. Phys.* **34** 2371
[39] Ivanov M and Corkum P 1993 *Phys. Rev. A* **48** 580
[40] Geng J W, Qin L, Li M, Xiong W H, Liu Y Q, Gong Q H and Peng L Y 2014 *J. Phys. B: At. Mol. Opt. Phys.* **47** 204027
[41] Tu X H, Hao X L, Li W D, Hu S L and Chen J 2016 *Chin. Phys. Lett.* **33** 93201
[42] Xie H, Li M, Luo S Q, Li Y, Zhou Y M, Cao W and Lu P X 2017 *Phys. Rev. A* **96** 063421